Molecular Therapy
Original Article

Full-length dystrophin restoration via targeted exon integration by AAV-CRISPR in a humanized mouse model of Duchenne muscular dystrophy

Adrian Pickar-Oliver,[1,2,3] Veronica Gough,[1,2,3] Joel D. Bohning,[1,2,3] Siyan Liu,[2,3,4] Jacqueline N. Robinson-Hamm,[1,3] Heather Daniels,[1,2,3] William H. Majoros,[3,5,6] Garth Devlin,[7] Aravind Asokan,[1,2,7,8] and Charles A. Gersbach[1,2,3,4,7,8,9]

[1]Department of Biomedical Engineering, Room 1427 FCIEMAS, 101 Science Drive, Box 90281, Duke University, Durham, NC 27708, USA; [2]Center for Advanced Genomic Technologies, Duke University, Durham, NC 27708, USA; [3]Center for Genomic and Computational Biology, Duke University, Durham, NC 27708, USA; [4]Graduate Program in Computational Biology and Bioinformatics, Duke University, Durham, NC 27708, USA; [5]Center for Statistical Genetics and Genomics, Duke University, Durham, NC 27708, USA; [6]Division of Integrative Genomics, Department of Biostatistics and Bioinformatics, Duke University School of Medicine, Durham, NC 27710, USA; [7]Department of Surgery, Duke University School of Medicine, Durham, NC 27710, USA; [8]Regeneration Next Initiative, Duke University, Durham, NC 27710, USA; [9]Department of Cell Biology, Duke University Medical Center, Durham, NC 27710, USA

Targeted gene-editing strategies have emerged as promising therapeutic approaches for the permanent treatment of inherited genetic diseases. However, precise gene correction and insertion approaches using homology-directed repair are still limited by low efficiencies. Consequently, many gene-editing strategies have focused on removal or disruption, rather than repair, of genomic DNA. In contrast, homology-independent targeted integration (HITI) has been reported to effectively insert DNA sequences at targeted genomic loci. This approach could be particularly useful for restoring full-length sequences of genes affected by a spectrum of mutations that are also too large to deliver by conventional adeno-associated virus (AAV) vectors. Here, we utilize an AAV-based, HITI-mediated approach for correction of full-length dystrophin expression in a humanized mouse model of Duchenne muscular dystrophy (DMD). We co-deliver CRISPR-Cas9 and a donor DNA sequence to insert the missing human exon 52 into its corresponding position within the DMD gene and achieve full-length dystrophin correction in skeletal and cardiac muscle. Additionally, as a proof-of-concept strategy to correct genetic mutations characterized by diverse patient mutations, we deliver a superexon donor encoding the last 28 exons of the DMD gene as a therapeutic strategy to restore full-length dystrophin in >20% of the DMD patient population. This work highlights the potential of HITI-mediated gene correction for diverse DMD mutations and advances genome editing toward realizing the promise of full-length gene restoration to treat genetic disease.

INTRODUCTION

Genome-editing technologies provide exciting potential for treating genetic disease.[1] Specifically, the RNA-guided clustered regularly interspaced short palindromic repeats (CRISPR)-Cas9 genome-editing system can be targeted to directly and precisely cleave genomic DNA and stimulate DNA repair by various mechanisms.[2–6] The resulting double-strand breaks (DSBs) in DNA stimulate the error-prone nonhomologous end-joining (NHEJ) repair pathway that leaves small insertion or deletion mutations (indels) at the target site. These indels can be used for gene knockout strategies by shifting the reading frame and introducing premature stop codons. Additionally, genomic deletions can be generated when two nucleases are simultaneously targeted to a region to remove the sequence between two DSBs. Alternatively, a DNA repair template can be delivered with Cas9 to stimulate the homologous recombination-mediated repair (HDR) pathway. This repair mechanism can be used to introduce a specific change in the targeted genomic site, such as generating a nucleotide substitution or a targeted DNA insertion. The various DSB repair mechanisms can be utilized for a wide range of gene therapy strategies.

Targeted DNA insertion approaches are typically based on the HDR pathway,[7–10] but this strategy is inefficient and limited to dividing cells.[11] Alternatively, site-specific integration frequencies in both dividing and non-dividing cells have been improved using an NHEJ-based method for targeted integration of linear double-stranded DNA.[12,13] The CRISPR-Cas9-mediated homology-independent targeted integration (HITI) strategy was originally demonstrated as a gene-replacement therapy using a rat model for retinitis pigmentosa.[14] Subretinal injection of HITI-AAV injection in a rat model led to correction of the *Mertk* gene by inserting a corrected copy of *Mertk* exon 2 upstream of a genomic deletion mutation. Recently, HITI-mediated reporter gene integration was reported in primary human

Received 17 May 2021; accepted 5 September 2021;
https://doi.org/10.1016/j.ymthe.2021.09.003.

Correspondence: Charles A. Gersbach, PhD, Department of Biomedical Engineering, Room 1427 FCIEMAS, 101 Science Drive, Box 90281, Duke University, Durham, NC 27708-0281, USA.
E-mail: charles.gersbach@duke.edu

CD34+ hematopoietic progenitor cells with long-term transgene expression following transplantation into immunodeficient mice.[15] These proof-of-principle studies demonstrate the exciting potential of HITI-based gene therapy approaches to correct genetic disease by targeted insertion strategies.

A primary target for gene therapy development is Duchenne muscular dystrophy (DMD). Occurring in ~1:5,000 newborn males, DMD is among the most prevalent fatal genetic diseases.[16] DMD is often fatal in the third decade of life as a result of progressive muscle weakness due to a lack of functional dystrophin protein in skeletal and cardiac muscle cells.[17] In these cells, dystrophin is an important structural element that functions to anchor proteins between the cytoskeleton and muscle fiber membrane. A lack of functional dystrophin is caused by mutations that disrupt the translational reading frame or create a premature stop codon in the X-linked *DMD* gene. This gene is susceptible to a high sporadic mutation rate due to its large size of 79 exons that cover over 2.3 million bp,[18] as well as repetitive elements that make the gene susceptible to recombination, leading to deletions of one or more exons. Because DMD is monogenic, prevalent, and fatal, it is an important candidate for gene therapy development.

The large size of the 14-kb dystrophin transcript makes conventional gene delivery strategies difficult. Consequently, commonly pursued therapeutic strategies aim to generate expression of a truncated but partially functional dystrophin protein that is similar to the product of the *DMD* gene in Becker muscular dystrophy (BMD), which is associated with milder symptoms relative to DMD. These approaches include delivery of mini- or micro-dystrophin genes[19–23] and oligonucleotide-mediated exon-skipping strategies in which a DMD deletion is extended to restore the correct reading frame.[24,25] Genome editing for DMD offers the potential of a one-time treatment that permanently restores a large fraction of the endogenous gene sequence in its natural position in the chromosomal DNA.[26] Numerous genome-editing approaches for correcting DMD have been explored for targeting CRISPR-Cas9 to edit the *DMD* gene. In ~60% of DMD patients, deletions in the mutational hotspot around exons 45–55 disturb the translational reading frame.[27] Several groups have restored the reading frame with NHEJ-mediated genome-editing approaches that excise or exclude additional exons around the inherited deletion. Targeted exon deletions generated in this region have shown mouse dystrophin restoration in mouse models,[28–34] canine dystrophin restoration in a canine model,[35] and human dystrophin restoration in patient-derived myoblasts,[36,37] patient-derived pluripotent stem cells,[27,38] and humanized mouse models. However, although truncated dystrophin proteins have the potential to convert the DMD phenotype to the milder phenotype of BMD patients, they do not fully recapitulate the function of full-length dystrophin.[39] There remains a need to develop gene-editing strategies to restore the complete, fully functional dystrophin protein.

In this study, we developed AAV-based, HITI-mediated gene-editing therapies for correcting full-length human dystrophin. We used a dual AAV delivery system to express Cas9 and guide RNAs (gRNAs) for generating a targeted genomic DSB and to deliver donor templates for NHEJ-mediated integration at the cut site. To assess the therapeutic potential of this corrective therapy, we performed local intramuscular and systemic intravenous injections to evaluate full-length human dystrophin protein restoration in a humanized mouse model of DMD that contains the full-length human DMD gene but a frame-disrupting deletion of exon 52 on the dystrophin null *mdx* mouse background (hDMDΔ52/*mdx*). By delivering donor vectors to insert either the missing human exon 52 or a superexon encoding the complete human dystrophin cDNA sequence downstream of exon 51, we achieved full-length dystrophin restoration in skeletal and cardiac muscles. We used a high-throughput unbiased sequencing approach to characterize and quantify gene-editing outcomes in genomic DNA and cDNA transcripts. These HITI-based CRISPR gene-editing strategies could potentially be effective therapies to restore full-length dystrophin for >20% of the DMD patient population and could be extended to an even broader population.

RESULTS

Correction strategy for humanized mouse model of DMD

The hDMD/*mdx* mouse lacks mouse dystrophin due to the hallmark *mdx* mutation but produces human dystrophin from the full-length human *DMD* (*hDMD*) gene on mouse chromosome 5.[40] These mice can be used to generate humanized DMD mouse models by removing *hDMD* exons known to be missing in patient populations and thus eliminating all dystrophin expression.[41,42] Importantly, these humanized models can be used to test therapeutic strategies because human dystrophin restoration can functionally compensate for the lack of mouse dystrophin.[40] To study various gene-editing therapeutic strategies, we generated a hDMDΔ52/*mdx* mouse model by delivering *Streptococcus pyogenes* Cas9 (SpCas9) and gRNAs to hDMD/*mdx* zygotes for targeted exon 52 deletion from the *hDMD* gene. Deletion of exon 52 results in an out-of-frame mutation (Figure 1A) that creates a premature stop codon and subsequent loss of dystrophin expression. To restore full-length dystrophin expression, we developed a HITI-based approach to insert exon 52 at its corresponding position in the hDMD gene in this humanized hDMDΔ52/*mdx* mouse model. This dual AAV vector approach includes one AAV vector that encodes a *Staphylococcus aureus* Cas9 (SaCas9)[43] expression cassette and a second AAV vector that encodes a gRNA expression cassette with the exon 52 donor sequence (Ex52) flanked by the same gRNA target site found in intron 51 of the *hDMD* gene. Following co-delivery of both AAV vectors, Cas9 and the gRNA will be expressed and create a DSB at the genomic target site, as well as liberate the Ex52 donor sequence from the AAV vector so that, following NHEJ-based repair, the exon 52 sequence will integrate into the target site and restore a full-length dystrophin gene. Importantly, the gRNA target sites are in opposite orientation in the genomic DNA and AAV vector so that correct donor integration will disrupt the gRNA target sequence and prohibit further Cas9-based editing (Figure 1A).

Screening and validation of HITI-mediated integration

The specificity of DNA cleavage by the CRISPR-Cas9 system is critical to ensuring the safety and efficacy of this approach. To minimize potential off-target effects, bioinformatic analysis was used to design

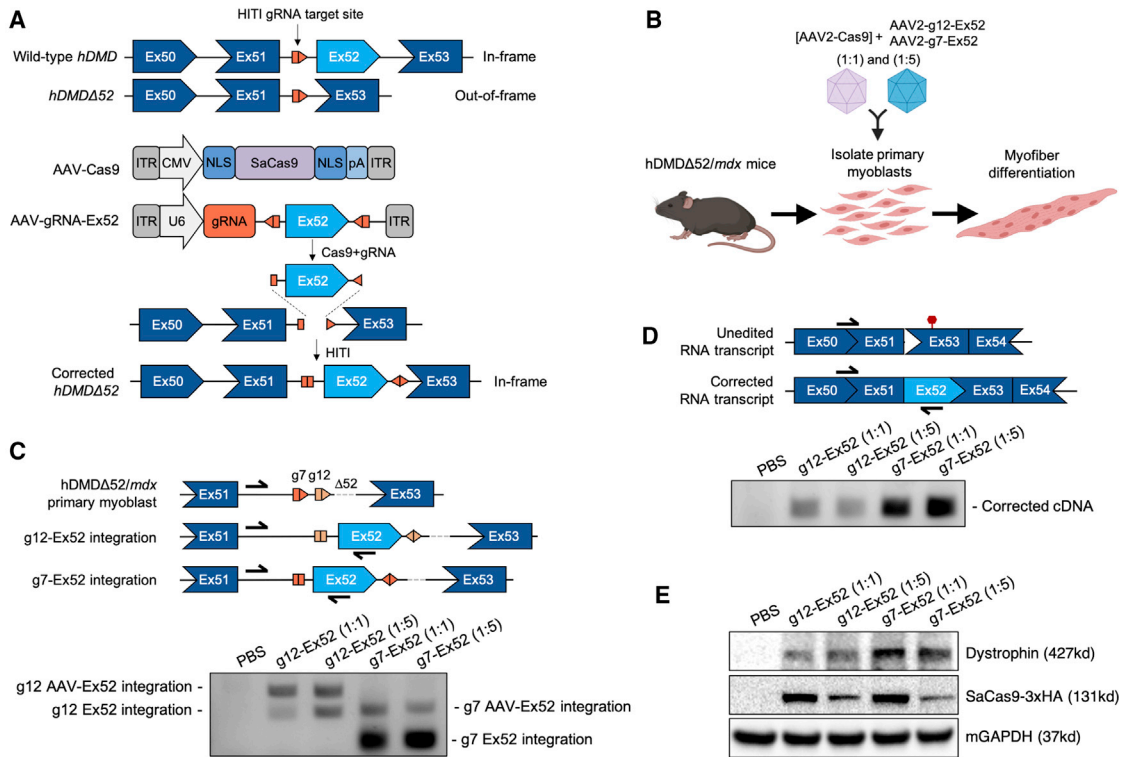

Figure 1. HITI-mediated exon 52 insertion restores full-length dystrophin in humanized hDMDΔ52/*mdx* primary myofibers

(A) Schematic of dual AAV vector approach for HITI-based exon 52 integration and correction of *hDMDΔ52* mutation. Orange pentagon, Cas9/gRNA target sequence; orange triangle, Cas9 cleavage site with PAM. (B) Primary myoblasts were isolated from hDMDΔ52/*mdx* skeletal muscle, co-transduced with AAV2 vectors at 1:1 and 1:5 (Cas9:gRNA-donor) vector genome ratios, and differentiated into myofibers. (C) Validation of correct gene knockin by genomic PCR is shown. (D) Validation of correct donor mRNA splicing by cDNA PCR is shown. (E) Western blot for dystrophin and Cas9 shows restoration of full-length dystrophin expression.

gRNAs with limited predicted off-target sites in murine and human genomes.[44] We screened a panel of SaCas9 gRNAs targeting intron 51 (Figure S1A; Table S1) to identify targets with high specificity and activity, initially using the Surveyor assay following plasmid transfection of HEK293T cells (Figure S1B). SaCas9 activity can vary across a range of spacer lengths;[43,45] therefore, we generated 19- to 23-nt spacers of our top gRNAs and individually screened them for activity by Surveyor assay, following plasmid electroporation into DMD patient myoblasts (Figure S1C). The individual gRNA sequences with the highest activity levels and fewest predicted off-target sites (g12 and g7), along with a scrambled non-target control gRNA (gScbl), were cloned into AAV vector plasmids for gRNA expression, and the corresponding spacer and PAM target sequences were included, flanking the donor sequence.

To validate targeted integration of the Ex52 donor sequence, primary myoblasts were isolated from hDMDΔ52/*mdx* skeletal muscle (Figure 1B). Following electroporation of AAV plasmids, targeted Ex52 integration in genomic DNA (gDNA) was confirmed by Sanger sequencing of the PCR-amplified genome-donor junction for g12-Ex52- and g7-Ex52-treated hDMDΔ52/*mdx* primary myoblasts, but not gScbl-treated cells (Figure S1D). To validate AAV-mediated targeted integration and subsequent correction of dystrophin transcripts and protein restoration, we transduced primary myoblasts with AAV2 and then cultured the cells in differentiation conditions to upregulate dystrophin expression (Figure 1B). In addition to delivering both AAV2 constructs at equal doses (1:1), we also tested delivery of 5× more AAV donor than AAV-Cas9 (1:5). Total volume of AAV preps remained consistent for 1:1 and 1:5 treatment groups, resulting in delivery of more AAV-Cas9 viral genomes for the 1:1 treatment group. Using both delivery ratios, targeted Ex52 integration was confirmed in gDNA by PCR amplification of the genome-donor junction (Figure 1C). We also detected the presence of a larger amplicon, which we confirmed to be intact AAV-donor integration by Sanger sequencing (data not shown). Additionally, the presence of Ex52 was observed in dystrophin cDNA following PCR amplification (Figure 1D) and resulted in dystrophin protein restoration (Figure 1E). The higher Cas9 expression observed in 1:1 treated cells correlates with the higher AAV-Cas9 viral dose. These results confirm activity of our AAV-Cas9-based strategy for targeted Ex52 integration and full-length dystrophin protein restoration.

AAV-Cas9 exon 52 integration restores full-length dystrophin *in vivo*

We used AAV9 for delivery of the CRISPR-Cas system to hDMDΔ52/*mdx* mouse skeletal and cardiac muscle.[46] Following co-injection of

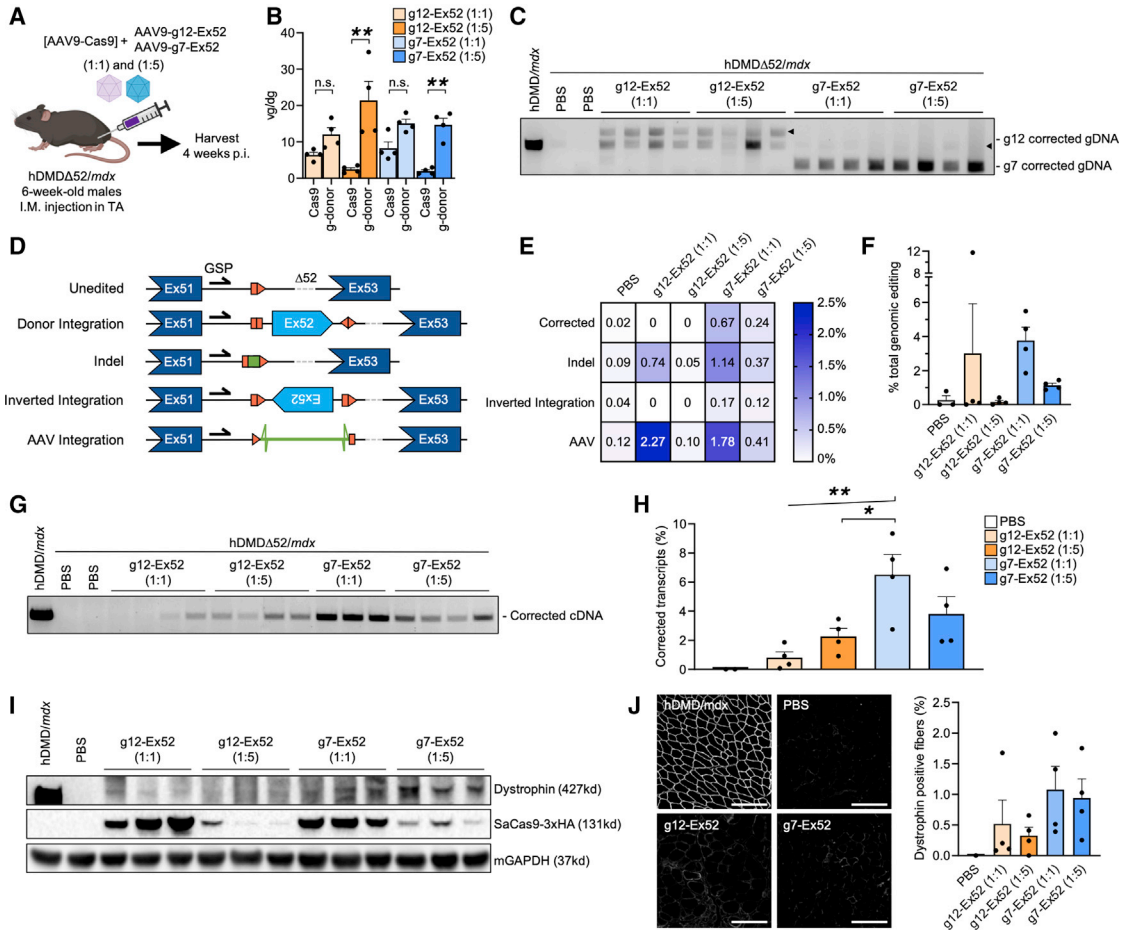

Figure 2. AAV-CRISPR-targeted exon 52 integration restores full-length dystrophin in hDMDΔ52/*mdx* mouse skeletal muscle

(A) Adult hDMDΔ52/*mdx* male mice were co-injected in TA muscles with AAV9 vectors at 1:1 and 1:5 (Cas9:gRNA-donor) vector genome ratios. (B) No significant differences in AAV viral genomes per diploid genomes (vg/dg) quantification in TA tissue between corresponding treatment groups are shown. (C) Validation of correct gene knockin in TA tissue by genomic PCR is shown. Black triangle, detected intact AAV-donor integration. (D) Schematic of potential on-target genomic edits that resulted from targeted DNA cleavage is shown. (E) Unbiased Tn5 tagmentation-based sequencing analysis of the various on-target genomic edits in TA tissues is shown. (F) Unbiased Tn5 tagmentation-based sequencing quantification of total on-target genomic edits in TA tissues is shown. (G) Validation of correct donor mRNA splicing in TA tissue by cDNA PCR is shown. (H) Higher levels of corrected dystrophin transcripts in TA tissue for g7-Ex52-treated mice quantified by ddPCR are shown. (I) Western blot for dystrophin and Cas9 expression shows restoration of dystrophin expression. (J) Dystrophin immunofluorescence staining shows a greater percentage of dystrophin-positive fibers in g7-Ex52-treated mice (scale bar, 200 μm; each dot represents mean of 5 images per mouse). One-way ANOVA, followed by Tukey's post hoc multiple comparisons test (**$p < 0.01$ and *$p < 0.05$; mean ± SEM; n = 4 mice).

the two AAV vectors into the tibialis anterior (TA) muscle of adult hDMDΔ52/*mdx* male mice (Figure 2A), we confirmed local AAV vector delivery at comparable levels for both g12 and g7 vectors by digital droplet PCR (ddPCR) of DNA vector genomes (Figure 2B). For all treated mice, targeted Ex52 integration and intact AAV-donor integration were confirmed in gDNA from TA tissue by PCR amplification of the genome-donor junction (Figure 2C). To quantify editing activity and comprehensively map possible genome-editing outcomes with an unbiased approach, we adapted Tn5-transposon-based library preparation methods[47,48] and included unique molecular identifiers (UMIs) to remove PCR duplicates for increased accuracy of quantifying rare events. The Tn5-based method eliminates PCR biases associated with target specificity and amplicon length by using a single genome-specific primer (GSP) adjacent to a gRNA cut site in combination with a transposon-specific primer for the Tn5-integrated DNA tag. In addition to quantifying donor integrations in the correct orientation, we measured genome-editing events that include indels, donor inversion integrations, and AAV-ITR integrations (Figure 2D). We measured higher correction and total genomic editing events in g7-treated mice (Figures 2E, 2F and S2). Indel and AAV integration edits were observed in both g7- and g12-treated mice (Figures 2E and S2). Although corrected genomic reads were not detected in g12-treated mice, the presence of exon 52 was observed in corrected dystrophin cDNA following PCR amplification (Figure 2G) and quantified by ddPCR (Figure 2H) for all treatment groups. Full-length dystrophin restoration was confirmed by western

blot of whole TA tissue lysates (Figure 2I), and dystrophin-positive fibers were quantified by immunofluorescence (IF) (Figure 2J). These results confirm *in vivo* activity of our AAV-Cas9-based strategy for targeted Ex52 integration and full-length dystrophin protein restoration following local injection in hDMDΔ52/*mdx* mouse skeletal muscle.

Assessing CRISPR-Cas targeting specificity is important for pre-clinical development. Collectively, greater genome-editing activity and subsequent dystrophin restoration was measured for g7-treated mice (Figure 1); thus, we focused our specificity analyses on g7. To empirically determine the top g7 off-target sites in the human genome with an unbiased genome-wide assay, we performed high-throughput genome-wide editing quantification (Figure S3).[49,50] These analyses identified 6 potential off-target sites with editing activity $\leq$1.07% of on-target gDNA editing, confirming high specificity of this g7 gRNA. Deep sequencing of 5 of these sites (OT1–5) in transfected HEK293T cells did not detect any editing above the detection limit of ~0.2% in untreated controls; 1 of the sites (OT6) was not amplifiable by PCR. For the remainder of our work, we focused on g7-targeted, full-length dystrophin restoration strategies.

In vitro validation of AAV-Cas9 superexon strategy for full-length dystrophin restoration

The g7-Ex52 integration approach can correct full-length dystrophin for Δ52 DMD patients and restore the proper reading frame to produce a truncated dystrophin protein for Δ52–58, Δ52–61, and Δ52–76 patient mutations. To expand the full-length dystrophin correction strategy to treat any genetic mutation downstream of exon 51, we engineered an AAV-superexon donor vector. This superexon encodes the complete dystrophin cDNA coding sequence downstream of exon 51, including exons 52 through 79. Additionally, we replaced the stop codon with a 3× stop to ensure translation termination in all reading frames, included the SV40 polyA sequence, and flanked the donor cassette with the previously validated g7 target sites (Figure 3A). Targeted integration of this g7-superexon construct could correct full-length dystrophin in >20% of all DMD patients.[51,52]

To validate superexon integration and subsequent correction of dystrophin transcripts and protein restoration, we transduced primary myoblasts with AAV2 at 1:1 and 1:5 vector ratios and then cultured the cells in differentiation conditions to upregulate dystrophin expression (Figure 3B). Targeted integration was confirmed in gDNA by PCR amplification of the genome-donor junction for all treated samples, in addition to detection of intact AAV-donor integration (Figure 3C). The presence of exon 52 from both donors was observed at comparable levels in dystrophin cDNA following PCR amplification (Figure 3D). For wild-type dystrophin transcripts, almost 2.7 kb of untranslated region (3′ UTR) is included in exon 79 following the stop codon. In the superexon donor, we replaced this sequence with a shortened polyA signal due to the packaging size restrictions of AAV (~4.7 kb). To characterize this engineered 3′ UTR, we performed 3′ rapid amplification of cDNA ends (RACE) using cDNA of AAV-transduced cells and amplified superexon-corrected dystrophin transcripts using a GSP that recognizes the engineered 3× stop (Figure 3E). Following Sanger sequencing, we observed addition of a polyA tail within the SV40 polyA signal sequence. Next, we confirmed that superexon-corrected dystrophin transcripts resulted in dystrophin protein restoration (Figure 3F). These results confirm activity of this targeted AAV-Cas9-based Ex52–79 superexon integration strategy for full-length dystrophin protein restoration.

AAV-Cas9 superexon strategy restores full-length dystrophin in skeletal muscle and cardiac muscle

To test the superexon strategy *in vivo*, we co-injected our AAV9 constructs at a ratio of 1:1 and 1:5 into the TA muscle of adult hDMDΔ52/*mdx* male mice (Figure 4A). We included a scrambled non-target gRNA donor (gScbl-Ex52) as an additional control. At 8 weeks post-injection, we measured equivalent AAV vector genome levels between treatment groups by ddPCR (Figure 4B). Targeted editing activity was quantified using Tn5-based library preparation and analysis methods with the highest editing levels in the 1:5 treated mice. The lower g7-Ex52 editing levels observed in this donor comparative study (Figures 4C and S4), in contrast to the previous gRNA comparative study (Figures 2E and S2), are likely due to lower AAV transduction in the TA as demonstrated by differences in vector genome quantification (Figures 2B and 4B). Although corrected gDNA levels were not detected above background by Tn5 analysis, we observed an increase in the percent of corrected transcripts for all treatment groups (Figure 4D). Additionally, full-length dystrophin expression was observed by western blot (Figure 4E) and IF (Figure 4F), and quantification of dystrophin-positive fibers resulted in a significant increase for g7-Ex52-treated mice compared to the scrambled non-targeted donor control. These results confirm *in vivo* activity of this AAV-Cas9-based strategy for targeted superexon integration and full-length dystrophin protein restoration following local injection in hDMDΔ52/*mdx* mouse skeletal muscle.

Next, we evaluated the corrective therapeutic potential of these integration strategies following systemic delivery. For transduction of cardiac and skeletal muscle, we co-delivered the AAV9 constructs at a ratio of 1:1 and 1:5 by facial vein injection of postnatal day 2 (P2) neonate hDMDΔ52/*mdx* male mice (Figure 5A). At 8 weeks post-injection, vector genome quantification by ddPCR revealed higher transduction levels in cardiac tissue than skeletal (diaphragm and TA) tissues (Figure 5B), suggesting the potential for higher editing activity in hearts of treated mice. Indeed, Tn5-based quantification revealed higher editing for all quantified outcomes in the heart gDNA compared to diaphragm and TA, with the highest on-target gDNA correction >3% in hearts of g7-superexon treatment groups (Figure 5C) with 4%–7% gDNA correction in four mice (Figure S5). We also observed higher levels of corrected dystrophin transcripts in hearts of g7-superexon treatment groups with mice achieving >25% corrected transcripts (Figure 5D). Our ddPCR-based transcript quantification is limited to detection of unedited (Ex51-Ex53 junction) and corrected (Ex51-Ex52 junction) cDNA molecules. For additional heart transcript characterization, we measured putative aberrant splicing events that

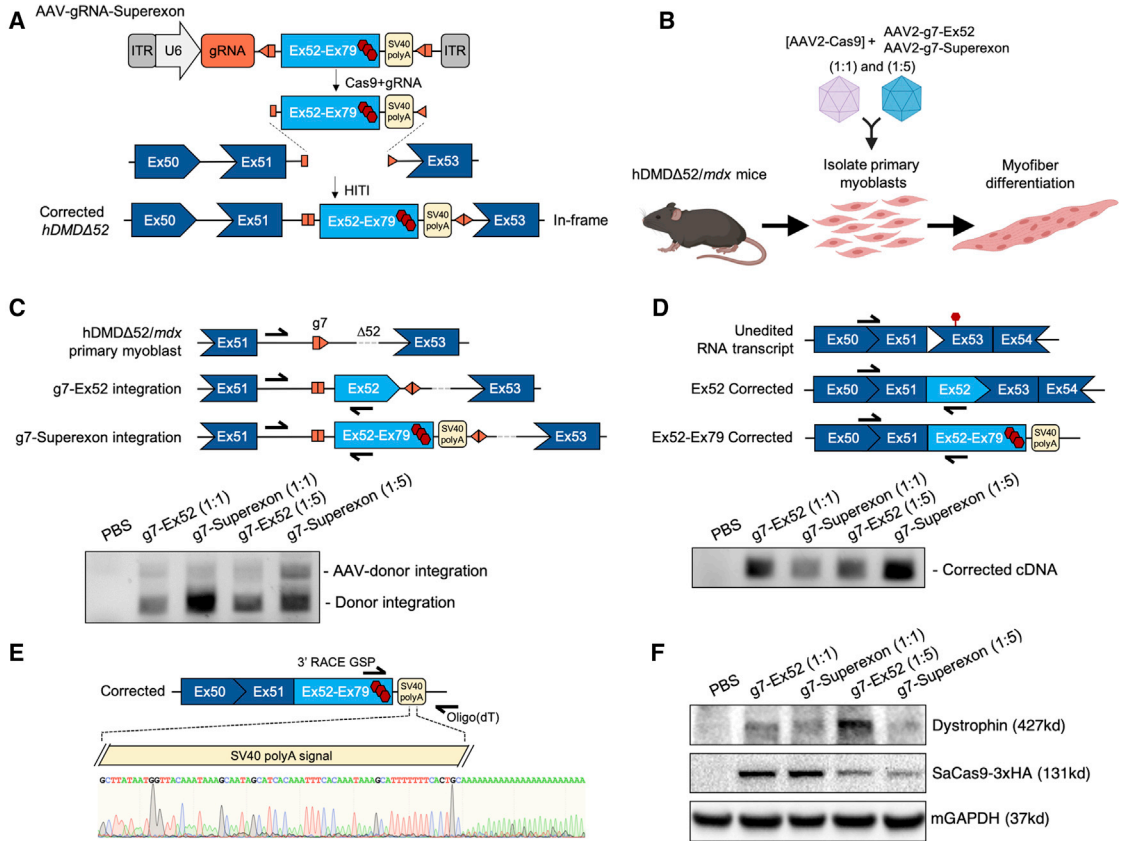

Figure 3. HITI-mediated superexon insertion restores full-length dystrophin in humanized hDMDΔ52/*mdx* primary myofibers

(A) Schematic of dual AAV vector approach for HITI-based superexon integration and correction of *hDMDΔ52* mutation. Orange pentagon, Cas9/gRNA target sequence; orange triangle, Cas9 cleavage site with PAM; red hexagon, stop codon. (B) Primary myoblasts were isolated from hDMDΔ52/*mdx* skeletal muscle, co-transduced with AAV2 vectors at 1:1 and 1:5 (Cas9:gRNA-donor) vector genome ratios, and differentiated into myofibers. (C) Validation of correct gene knockin by genomic PCR is shown. (D) Validation of correct donor mRNA splicing by cDNA PCR is shown. (E) Characterization of Superexon-corrected polyA tail using 3′ RACE with genome-specific primer (GSP) for 3× stop is shown. (F) Western blot for dystrophin and Cas9 shows restoration of dystrophin expression for Ex52- and superexon-treated samples.

include inversion donor integrations, splicing with the SaCas9 coding sequence, circular RNA formation (exons 1–51), multi-exon skipping (exons 53–79), and alternative splicing with downstream intronic sequences (introns 51–53; Figure 5E). Consistent with previous work from our group, higher levels of editing were measured by ddPCR than Tn5-based deep sequencing strategies.[47] Lower deep sequencing editing percentages may be attributed by larger denominators generated from measuring unintended gene editing outcomes. For cDNA analysis, our high-throughput deep sequencing characterization revealed considerable aberrant splicing with the SaCas9 coding sequence in two treated mice (Figure S6A). Upon further investigation, we confirmed genomic integration of aligned sequences in corresponding genomic mouse samples (Figure S6B). Transcript isoforms that contain partial AAV genomes, including partial SaCas9 coding sequences, have an unknown biological effect and could be investigated in future studies. In heart tissue, full-length dystrophin restoration was confirmed by western blot (Figure 5F) and dystrophin-positive cells were detected in all treated mice (Figures 5G and S7). A significant increase in dystrophin-positive cells was observed for g7-superexon (1:1)-treated mice compared to the scrambled non-targeted gRNA donor control, with almost 50% of dystrophin-positive cells observed for one mouse. Serum creatine kinase levels, a marker of muscle degeneration, were significantly higher for control hDMDΔ52/*mdx* mice compared to hDMD/*mdx* mice, suggestive of a diseased DMD phenotype (Figure 5H). Additionally, serum creatine kinase levels were reduced in hDMDΔ52/*mdx* mice after all systemic treatments, demonstrating protection from muscle damage by the restored full-length dystrophin protein.

DISCUSSION

DMD gene therapy strategies have been explored for nearly 30 years;[18,53] however, strategies to correct full-length dystrophin are lacking. In this study, we demonstrate use of targeted HITI-mediated transgene insertion for full-length human dystrophin correction and restoration in hDMDΔ52/*mdx* mice. We used a dual AAV delivery system for generating a Cas9-targeted genomic DSB and delivering donor sequences for NHEJ-mediated integration at the cut site. Previously, NHEJ-mediated integration has been utilized for *in vivo*

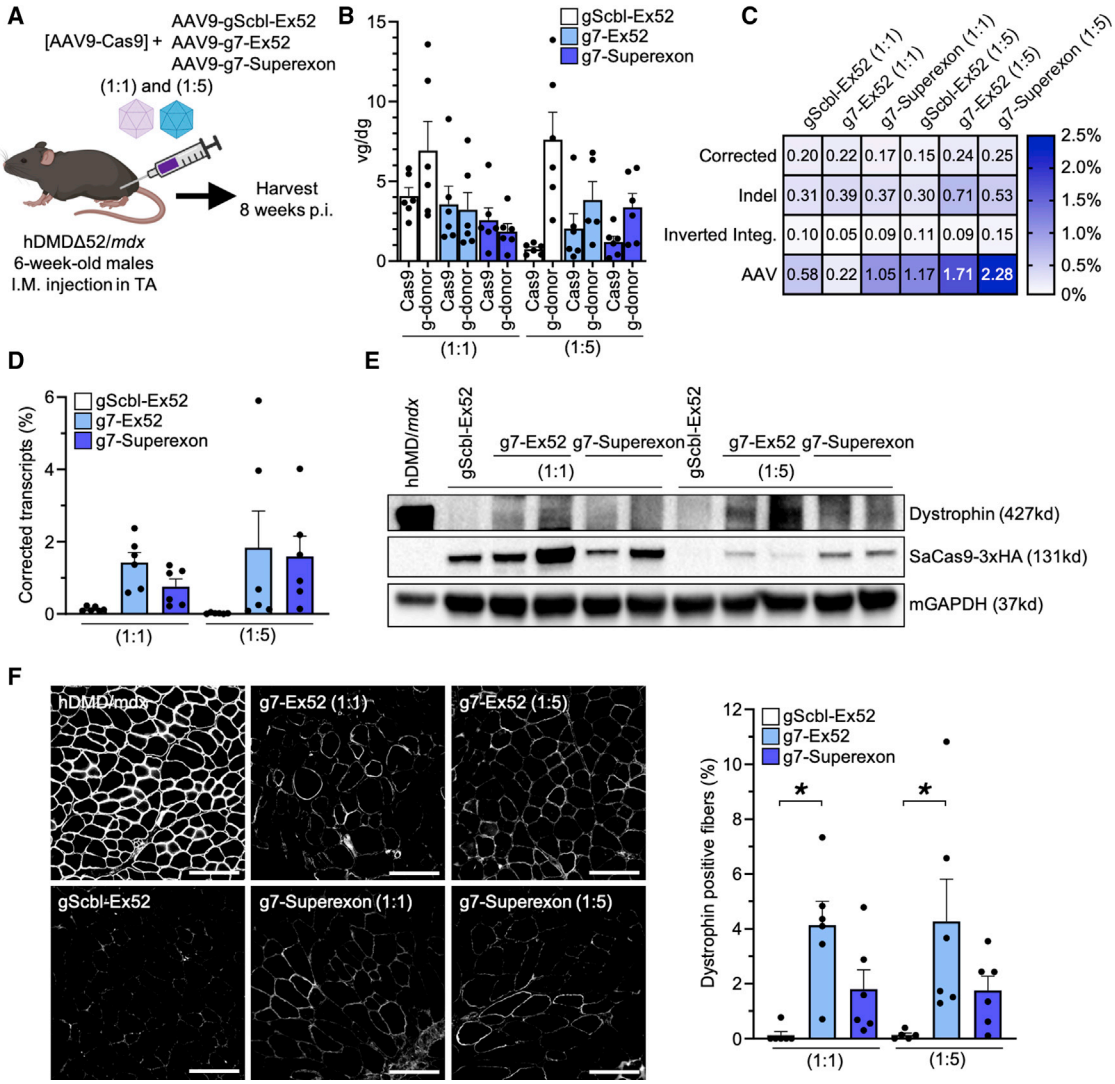

Figure 4. AAV-CRISPR-targeted superexon integration restores full-length dystrophin in hDMDΔ52/*mdx* mouse skeletal muscle

(A) Adult hDMDΔ52/*mdx* male mice were co-injected in TA muscles with AAV9 vectors at 1:1 and 1:5 (Cas9:gRNA-donor) vector genome ratios. (B) No significant differences in AAV vector genomes per diploid genomes (vg/dg) quantification in TA tissue between corresponding treatment groups are shown. (C) Unbiased Tn5 tagmentation-based sequencing analysis of the various on-target genomic edits in TA tissues is shown. (D) Quantification of corrected dystrophin transcripts in TA tissue by ddPCR is shown. (E) Western blot for dystrophin and Cas9 shows restoration of dystrophin expression. (F) Dystrophin immunofluorescence staining shows a significant increase in the percentage of dystrophin-positive fibers in g7-Ex52-treated mice compared to scrambled non-targeted donor control mice (scale bar, 200 μm; each dot represents mean of 5 images per mouse). One-way ANOVA, followed by Tukey's post hoc multiple comparisons test (**$p < 0.01$ and *$p < 0.05$; mean ± SEM; n = 6 mice).

proof-of-principle gene therapy approaches following AAV delivery in primary human CD34+ HSPCs[15] and following direct administration in the targeted tissue.[14] Here, we demonstrate the therapeutic potential of NHEJ-mediated integration approaches following both local injection and systemic delivery in skeletal and cardiac tissues. Additionally, we perform high-throughput unbiased sequencing to characterize and quantify genomic and transcriptional editing events.

Although downstream consequences of HITI-mediated correction resulted in dystrophin protein restoration, our deep sequencing results demonstrate low genomic correction efficiency. The observation of high dystrophin protein restoration resulting from low genomic editing efficiency is consistent with alternative DMD gene-editing approaches.[28,47] Although low levels of dystrophin expression, even less than 4% of normal, can result in potential therapeutic benefit,[54–56] improving HITI efficiency will aid translation of knockin gene therapy strategies to clinical applications. This gene-editing strategy is similar to other gene transfer strategies in its need for robust delivery to targeted tissues and cells. Additionally, humoral- and cellular-mediated host immune responses have been shown to

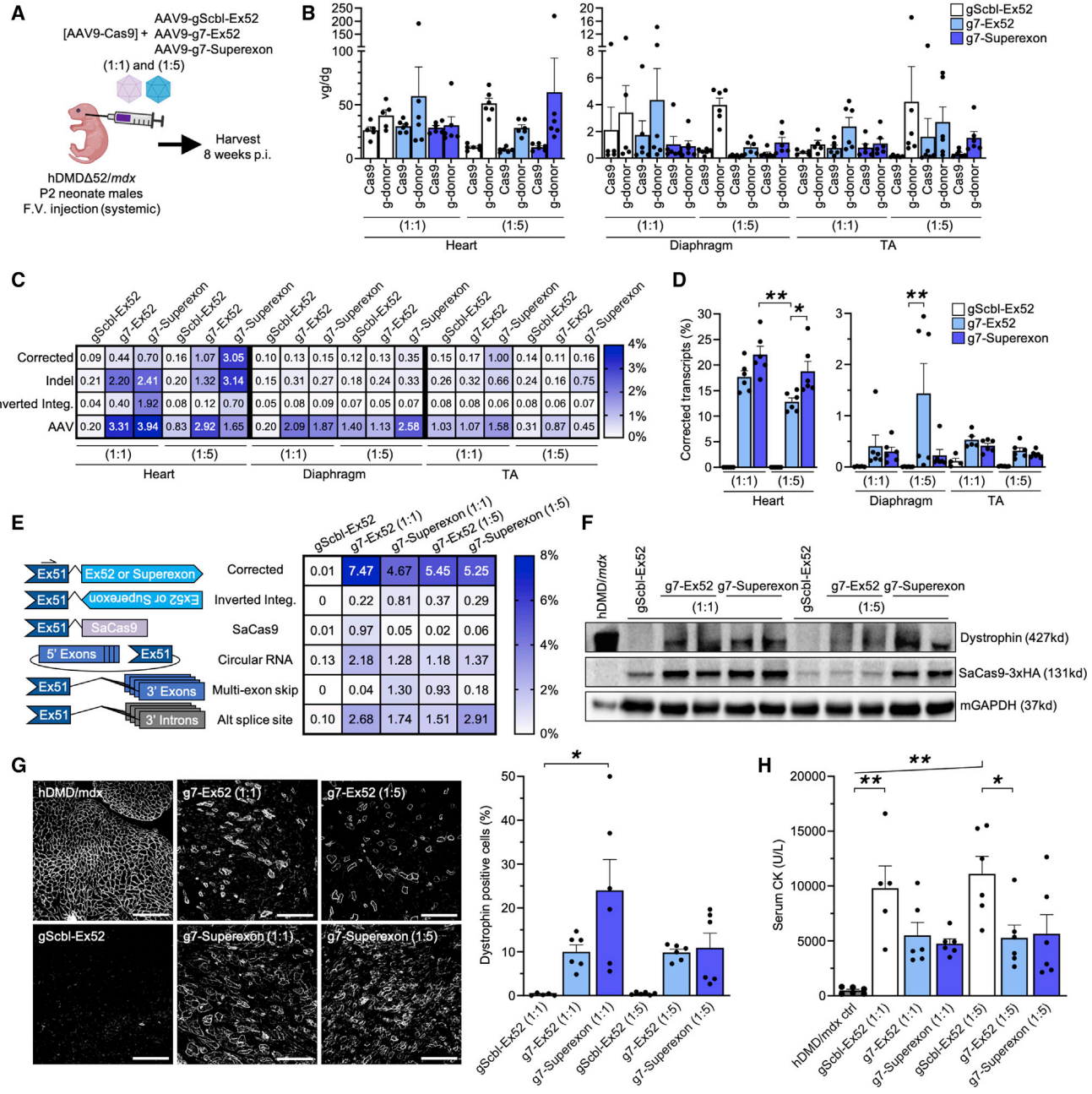

Figure 5. Systemic delivery of AAV-CRISPR-targeted integration strategies restores full-length dystrophin in hDMDΔ52/*mdx* mouse cardiac muscle

(A) Systemic facial vein co-injection in P2 neonate hDMDΔ52/*mdx* male mice with AAV9 vectors at 1:1 and 1:5 (Cas9:gRNA-donor) vector genome ratios. (B) No significant differences in AAV vector genomes per diploid genomes (vg/dg) quantification in cardiac (heart) or skeletal (diaphragm and TA) tissue between corresponding treatment groups are shown. (C) Unbiased Tn5 tagmentation-based sequencing analysis of the various on-target genomic edits shows corrected integration at levels above background in cardiac tissue. (D) Higher levels of corrected dystrophin transcripts in heart tissue for treated mice quantified by ddPCR are shown. (E) Unbiased Tn5 tagmentation-based sequencing analysis of the various on-target heart cDNA shows diverse transcript outcomes, including aberrant splicing. (F) Western blot for dystrophin and Cas9 shows restoration of dystrophin expression in heart tissue. (G) Dystrophin immunofluorescence staining in heart tissue shows detection of dystrophin-positive fibers in all treated mice, with a significant increase in the percentage of dystrophin-positive fibers in g7-superexon (1:1)-treated mice compared to scrambled non-targeted donor control mice (scale bar, 200 μm; each dot represents mean of 5 images per mouse). (H) Serum creatine kinase levels show a decrease in hDMDΔ52/*mdx*-treated mice compared to diseased hDMDΔ52/*mdx* scrambled non-targeted donor control mice. One-way ANOVA, followed by Tukey's post hoc multiple comparisons test (**$p < 0.01$ and *$p < 0.05$; mean ± SEM; n = 6 mice).

impact gene-editing activity.[47,57–59] Methods to circumvent host immunological responses and improve AAV-mediated, tissue-specific transduction and expression, such as AAV capsid evolution[60] and promoter engineering,[61] will ensure improvements in gene-editing activity and therapeutic potential. Additionally, targeted integration in dividing and non-dividing cells can be increased by identification of NHEJ regulators, leading to the development of small-molecule targets for enhancing HITI-mediated activity. Alternatively, other targeted gene knockin methods can be explored, including microhomology-mediated end-joining (MMEJ),[62] precise integration into target chromosome (PiTCh),[63–65] homology-mediated end joining (HMEJ),[66] and intercellular linearized single homology arm donor mediated intron-targeting integration (SATI).[67] With continued progress in editing efficiency, HITI-mediated transgene knockin holds great promise for future development of corrective gene therapy strategies.

Pre-clinical gene editing studies benefit from use of humanized mouse models because they permit testing of therapeutic approaches specifically designed to treat human patients. To apply HITI-based gene therapy strategies to a DMD disease model that recapitulates mutations found in patients, we utilized hDMDΔ52/*mdx* mice, which contain a gene deletion within the DMD patient mutational hotspot of exons 45–55.[27] We demonstrate full-length protein restoration following targeted integration of the missing exon 52 coding sequence. To expand this corrective gene therapy approach to a larger patient population (>20%), we engineered a superexon encoding the complete human dystrophin cDNA coding sequence downstream of exon 51 that can correct all patient mutations located after exon 51 and demonstrated full-length protein restoration using this approach. This work is the first demonstration of a targeted gene-editing approach to permanently correct full-length human dystrophin. Future efforts can expand this approach to all patients with mutations within and downstream the exon 45–55 hotspot (>50% of all patients) by developing a dual AAV-based system with one AAV that encodes SaCas9 and a gRNA targeting intron 44 and a second donor AAV vector that contains the human dystrophin cDNA coding sequence downstream of exon 44 (exons 45–79).

The engineered superexon donor encodes a shortened polyA signal to ensure proper transcriptional signals during mRNA generation from corrected genomic edits. The 3′ RACE characterization confirmed the addition of a polyA tail in superexon-corrected transcripts (Figure 2E). Future efforts aimed to engineer superexon donors with 3′ UTRs optimized for mRNA stability may result in enhanced therapeutic potential. HITI-mediated single exon and superexon gene-editing approaches can also be applied to other genetic diseases, including those with gene targets, like *DMD*, that are too large to fully package in AAV delivery vectors or characterized by a wide spectrum of patient mutations, including hemophilia, cystic fibrosis, and neurofibromatosis type 1.

Previously, proof-of-principle HITI-mediated gene-corrective strategies characterized editing outcomes by Surveyor analysis, in-out PCR amplification, ddPCR, and TOPO sequencing.[14,15] In this study, we also used Tn5-transposon-based library preparation methods and unbiased deep sequencing characterization for greater resolution of diverse HITI-mediated editing outcomes. Using these methods, we detected on-target genomic site-specific integration of intended donor corrections, inverted donor insertions, indels, AAV-ITR integrations, and AAV-Cas9 coding sequences. Analysis of cDNA edits demonstrated on-target intended splicing and aberrant splicing, including intended donor inclusion, inverted donor sequences, Cas9 coding sequences, circular RNAs, multi-exon skips, and alternative splice sites in downstream introns. These results are all consistent with our previous observations of unintended editing outcomes using AAV-CRISPR.[47] Although these unintended on-target editing outcomes are undesirable, it is not yet clear whether there is any negative biological consequence of these events. Moreover, our unbiased, genome-wide investigation of off-target editing activity showed ~1% or less DNA cutting at any off-target site relative to on-target activity in a highly sensitive *in vitro* digestion assay (Figure S3), and editing at these putative off-target sites was undetectable in transfected HEK293T cells. Continued efforts for unbiased characterization of genomic and transcriptional editing events are indispensable for future development of therapeutic gene-editing strategies and HITI-based approaches in particular. Although Tn5-based library preparation methods permit improved characterization of unintended edits, the Illumina sequencing methods are limited to short-read sequencing (~150–300 bp). Short read lengths do not permit full characterization of intact AAV-donor integrations; therefore, we are unable to confirm whether these editing events contain the full donor sequence and potentially contribute to full-length dystrophin expression. Additionally, we observed integration of AAV genome fragments, including partial SaCas9 coding sequences; however, any biological effect of these edits remains uncertain. Further characterization of AAV integration events will be informative for HITI and non-HITI AAV-CRISPR approaches. In future studies, long-read sequencing technologies could be combined with amplification-free targeted sequencing for complete characterization of full integrated sequences.

Gene-editing technologies have garnered incredible enthusiasm for the potential to correct genetic mutations to restore healthy, wild-type gene sequences. However, the majority of gene-editing strategies being advanced to clinical trials today involve gene disruption, activation of compensatory factors, introduction of therapeutic genes to non-native "safe-harbor" loci, or the creation of truncated, partially functional gene sequences.[68] This study, and others using similar approaches aimed to restore native genes, represents an important step toward realizing the full potential of genome editing to treat the fundamental cause of genetic disease.

MATERIALS AND METHODS

Plasmid design and AAV production

The ITR-containing *Staphylococcus aureus* Cas9 (pAAV-SaCas9) expression plasmid was generated by adding a 3xHA epitope to the carboxyl terminus of SaCas9[47] using Gibson cloning strategies. The

CMV-SaCas9-3xHA-polyA was transferred to a new plasmid (pSaCas9) without ITRs for stability in cell culture experiments. A separate plasmid with a hU6-driven guide RNA cassette[28] (pU6-gRNA) was used with BbsI cloning to screen guides *in vitro*. For AAV-gRNA-donor plasmids (pAAV-g12-Ex52, pAAV-g7-Ex52, and pAAV-g7-Superexon), gene blocks were synthesized by integrated DNA technology (IDT) and integrated into ITR-containing plasmids by Gibson cloning strategies. See Note S1 for pAAV plasmid sequences. Intact ITRs were verified by SmaI digest before AAV production on all vectors. Multiple batches of AAV2 and AAV9 were produced by the Duke University Viral Vector Core and by the Asokan laboratory at Duke University. Titers were measured by qPCR with a plasmid standard curve.

In vitro gRNA screening

A panel of gRNAs (Table S1), with predicted minimal off-target effects,[44] was designed to target intron 51 of the human DMD gene and compared for SaCas9 activity by Surveyor assay in HEK293T cells and DMD patient myoblasts. HEK293T cells were maintained in Dulbecco's modified Eagle's medium (DMEM) (Invitrogen) with 10% fetal bovine serum (FBS) (Sigma) and 1% penicillin-streptomycin (P/S) (Gibco). Immortalized DMD patient 8036 myoblasts (DM8036 cell line with a deletion of exons 48–50 in the *DMD* gene)[69] were maintained in skeletal muscle media (PromoCell) with 20% FBS (Sigma), 50 μg/mL fetuin (Sigma), 10 ng/mL human epidermal growth factor (Sigma), 1 ng/mL human basic fibroblast growth factor (bFGF) (Sigma), 10 μg/mL human insulin (Sigma), 400 ng/mL dexamethasone (Sigma), 1% GlutaMAX (Invitrogen), and 1% P/S. Cells were incubated at 37°C with 5% CO_2. HEK293T cells were transfected with 375 ng pSaCas9 and 125 ng pU6-gRNA plasmid using Lipofectamine 2000 (Invitrogen) according to the manufacturer's protocol. DMD myoblasts were electroporated with 10 μg pSaCas9 and 10 μg pU6-gRNA plasmid with a Gene Pulser XCell (Bio-Rad) in PBS using previously optimized conditions.[37] Cells were incubated for 72 h, and genomic DNA was isolated with a DNeasy kit (QIAGEN). Indels were identified by PCR of the region of interest (Surveyor primers provided in Table S2) performed using the Invitrogen AccuPrime High Fidelity PCR kit, following by incubation with the Surveyor Nuclease and electrophoresed on TBE gels (Life Technologies) as previously described.[28,70] In brief, percent editing was calculated by measuring the intensities of the unedited and edited amplicon bands. These values were used to calculate the percent of edited amplicon bands ([edited band 1 + edited band 2]/[total band intensities]) and then used to calculate percent editing using the following formula: (1 − [square root(1 − percent of edited amplicon bands)] × 100).

Animals

All experiments involving animals were conducted with strict adherence to the guidelines for the care and use of laboratory animals of the National Institutes of Health (NIH). All experiments were approved by the Institutional Animal Care and Use Committee (IACUC) at Duke University. The hDMD/mdx mouse[40] was kindly provided by Leiden University Medical Center. The generation of the hDMDΔ52/mdx mouse was completed by the Duke Transgenic Mouse Facility. Briefly, B6SJLF1/J donor females were superovulated by intraperitoneal injection of 5IU PMSG on day 1 and 5IU HCG on day 3, followed by mating with fertile hDMD/mdx males. On day 4, embryos were harvested and injected with mRNA encoding *S. pyogenes* Cas9 and gRNAs targeting human intron 51 (CTCTGAT AACCCAGCTGTGTGTT) and human intron 52 (CTAGACCAT TTCCCACCAGTTCT). Injected embryos were implanted into pseudo-pregnant CD1 female mice. Genomic DNA was extracted from ear punches of chimeric pups using the DNeasy Blood and Tissue Kit (QIAGEN) and screened for presence or deletion of exon 52. Mice with loss of exon 52 were bred with mdx mice. The resulting male hDMDΔ52/mdx (het;hemi) mice were used for experiments.

In vitro AAV transductions

Primary myoblasts were isolated from the TA and gastrocnemius muscles of hDMDΔ52/mdx mice, as previously described,[71] and maintained in F10 media (Invitrogen) supplemented with 20% FBS, 5 ng/mL bFGF, and 1% P/S. Cells were grown on plates coated with bovine type I collagen (Sigma) and incubated at 37°C with 5% CO_2. For transductions, cells were plated for 1.5 h and then AAV2-SaCas9 and AAV2-gRNA-donor vectors were combined and added to the plates at an MOI of 1×10^6 total vectors per cell. Cells were immediately spun at 3,000 × *g* for 5 min and returned to the incubator. Once cells reached 70% confluency, the media was changed to DMEM supplemented with 5% horse serum and 1% P/S and replaced every 2 days for differentiation into myofibers. Cells were differentiated for 10 days and processed for analysis of genomic DNA, total RNA, and protein as described.

Genomic DNA and RNA analysis from primary hDMDΔ52/*mdx* myoblasts

Genomic DNA was isolated using the DNeasy kit (QIAGEN) according to the manufacturer's protocol. Total RNA was isolated using QIAshredder and RNeasy Plus kits (QIAGEN). First-strand cDNA synthesis was performed using 500 ng total RNA per sample using the SuperScript VILO Reverse Transcription Kit (Invitrogen) and incubated at 25°C for 10 min, 42°C for 2 h, and 85°C for 5 min. Donor integration was detected by PCR (primers provided in Table S2) using the Invitrogen AccuPrime High Fidelity PCR kit according to the manufacturer's protocol and electrophoresed on 1% agarose gels. 3′ RACE was carried out on RNA samples using the SMARTer RACE 5′/3′ kit (Takara) for cDNA synthesis and primary PCR (primers provided in Table S2) using Program 1 according to the manufacturer's instructions.

In vivo AAV administration

Adult 6- to 8-week-old mice were administered AAV by intramuscular injection into the TA muscle with 40 μL PBS or AAV vector per mouse. For the donor comparative study, 1.56e12 total vg was administered to 1:1 treatment groups (7.81e11 AAV-Cas9 and 7.81e11 AAV-donor) and 2.13e12 total vg was administered to 1:5 treatment groups (3.55e11 AAV-Cas9 and 1.77e12 AAV-donor). For the gRNA comparative study, 8.64e11 total vg was administered

to the 1:1 treatment groups (4.32e11 AAV-Cas9 and 4.32e11 AAV-donor) and 7.00e11 total vg was administered to the 1:5 treatment groups (1.17e11 AAV-Cas9 and 5.83e11 AAV-donor). 2-day-old (P2) neonatal mice were administered AAV by intravenous injection through the facial vein[72] with 40 μL AAV vector per mouse. For the 1:1 treatment groups, 8.64e11 total vg was administered (4.32e11 AAV-Cas9 and 4.32e11 AAV-donor), and for the 1:5 treatment groups, 7.00e11 total vg was administered (1.17e11 AAV-Cas9 and 5.83e11 AAV-donor). At set time points, mice were euthanized and skeletal muscle, cardiac muscle, and serum were collected.

ddPCR

Quantitative ddPCR was performed on cDNA and gDNA samples using the QX200 Droplet Digital PCR system according to the manufacturer's instructions. To quantify corrected transcript levels, RNA was extracted from mouse tissues using the QIAGEN Universal kit. Subsequently, first-strand cDNA synthesis was performed using 500 ng total RNA per sample as stated above. Corrected hDMD transcripts containing exon 52 were detected using the QX200 ddPCR Supermix for Probes without dUTP (Bio-Rad) and Taqman assays with probes (Table S2) designed to bind to the human dystrophin Ex51–52 junction (corrected; ThermoFisher custom assay ID: AP2XDZ9), human dystrophin Ex51–53 junction (unedited; ThermoFisher custom assay ID: AP327K6), and human dystrophin Ex59–60 (input normalization; ThermoFisher custom assay ID: AP47Z63). Quantification was determined based on the number of positive droplets in each reaction using QuantaSoft Analysis software (Bio-Rad). cDNA input for corrected or unedited transcript levels was normalized by dividing the number of Ex51–52 or Ex51–53 of positive droplets, respectively, by the number of positive Ex59–60 droplets in each reaction. The percentage of corrected transcripts was calculated as (normalized Ex51–52) / ([normalized Ex51–52] + [normalized Ex51–53]) × 100. For vector genome quantification, gDNA was extracted from mouse tissues using the QIAGEN DNeasy kit and digested with HindIII-HF at 37°C for 1 h. Episomes were detected using the QX200 ddPCR Supermix for Probes without dUTP (Bio-Rad) and Bio-Rad assays with probes (Table S2) designed to bind SaCas9 (AAV-SaCas9; Bio-Rad unique assay ID: dCNS159380965), U6 (AAV-gRNA-donor; Bio-Rad unique assay ID: dCNS116676529), and mouse *EEF2* (input normalization; Bio-Rad unique assay ID: dMmuCNS781688813). Quantification was determined based on the number of positive droplets in each reaction using QuantaSoft Analysis software. Episome quantification was calculated as viral genomes per diploid genome (vg/dg) by dividing the number of SaCas9- or U6-positive droplets by the number of mouse *EEF2*-positive droplets in the corresponding reaction.

Transposon-mediated target enrichment and sequencing

Tn5 transposase protein was expressed and purified as previously described.[73] Tagmentation of genomic DNA was completed as previously described,[48] with the following modifications to include unique molecular indexes (UMIs). For RNA transcript analysis, first-strand cDNA synthesis was performed using 500 ng total RNA per sample as stated above. Second-strand synthesis was performed using Klenow fragment DNA polymerase (NEB) and purified using Ampure beads (Beckman Coulter) at 1.8×. All primer sequences are provided in Table S2. In brief, the linker oligonucleotides (Tn5-Top contains Illumina i7 adaptor sequence and 10 nucleotide UMI; Tn5-Bottom contains Tn5-ME sequence) were annealed and assembled on Tn5. Genomic DNA was quantified using NanoDrop (Thermo Fisher Scientific), and second-strand products were quantified using Qubit Fluorometric Quantification (Thermo Fisher Scientific). Tagmentation of 200 ng genomic DNA or second-strand products was performed using a 1:40 dilution of assembled Tn5 and purified using DNA Clean and Concentrator-5 columns or 96-well kits (ZymoGenetics). To enrich the targeted sequence, first-round PCR using a genome-specific primer (Tn5-GSP; contains custom adaptor) was used with a reverse primer (Tn5-Universal) specific for the i7 adaptor sequence inserted by the transposon for 25 cycles. Amplicons were purified with Ampure beads at 1.8×. Second-round PCR using a barcode primer (Tn5-BC) specific for the custom adaptor sequence was used to add 6-nt experimental barcodes, and the Illumina i5 adaptor was used with the Tn5-Universal reverse primer for 15 cycles. Amplicons were gel purified, followed by purification with Ampure beads at 0.6× to select for fragment sizes greater than 250 bp. Sequencing was conducted on an Illumina Miseq using 250- (read 1) and 50-cycle (read 2) paired-end reads with a custom read 1 primer (Tn5-Read1) or on an Illumina Novaseq v1.5 using 200-cycle single-end reads with a custom read 1 primer (Tn5-Read1) and custom index 1 primer (Tn5-Index1). The Tn5-based method is expected to reduce PCR-related bias from amplicon size; however, some bias may remain from the transposition selectivity.[48]

TSransposon-mediated target enrichment and sequencing

Demultiplex

Sequencing fastq files were demultiplexed using the list of barcodes for each sample.

Trim

The reads were trimmed for sequencing adapters and low-quality bases using Trimmomatic (v0.33).

Alignment and deduplication

Alignment of the trimmed reads was done using bwa-mem (v0.7.12) to the reference genomes (gDNA aligned to mouse genome GRCm38 + human *DMD*; cDNA aligned to human dystrophin cDNA). Aligned reads were tagged with their UMI using fgbio (v0.8.1) AnnotateBamWithUmis, and PCR duplicates were marked using Picard (v2.14.0) MarkDuplicates based on the UMI tag.

Alignment to reference sequences

Reference amplicons were built to align to the targeted locus and expected edits. To remove reads that are due to false priming, reads that do not contain the 20 bases directly adjacent to the GSP expected sequence were filtered out. To remove reads that do not extend far enough past the edit site, reads that are shorter than the required minimum length were filtered out. On-site deduplicated reads were aligned to reference amplicons using bwa-mem (v0.7.12). Aligned

reads were analyzed and identified based on editing outcomes using a custom-built script using python3 (https://github.com/siyansusan/DMD_integration_analysis). Reads that contain an indel ± 15 bp at the expected cut site or junction were identified. The number of distinct UMIs was counted for each edit to quantify frequency of editing events.

Western blot

Protein was isolated from muscle tissues by disruption with a BioMasher II Micro Tissue Homogenizer (VWR) in RIPA buffer (Sigma) with a protease inhibitor cocktail (Roche) and incubated for 30 min on ice with intermittent vortexing. Samples were spun at 16,000 × *g* at 4°C for 30 min, and supernatant was collected. Total protein was quantified using the BCA Protein assay kit (Pierce) according to the manufacturer's protocol and measured on a BioTek Synergy 2 Multi-Mode Microplate Reader. Sample was mixed with NuPAGE loading buffer (Invitrogen) and 5% β-mercaptoethanol, and 3.125 μg of hDMD/*mdx* protein or 25 μg of all other protein samples was heated at 100°C for 10 min. Samples were loaded into 4%–12% NuPAGE Bis-Tris gels (Invitrogen) with MES buffer (Invitrogen) and electrophoresed for 45 min at 200 V on ice. Protein was transferred to nitrocellulose membranes for 90 min in 1× tris-glycine transfer buffer with 0.01% SDS at 4°C at 400 mA. The blot was blocked in 5% milk-TBST (50 mM Tris, 150 mM NaCl, and 0.1% Tween-20) at 4°C overnight. Blots were cut and incubated with anti-MANDYS106 (1:50 dilution; Millipore clone 2C6), anti-HA (1:1,000 dilution; BioLegend clone 16B12), or anti-GAPDH (1:5,000 dilution; Cell Signaling Technology clone 14C10) in 5% milk-TBST at room temperature for 1 h. Blots were then washed in TBST and incubated with goat anti-mouse-conjugated horseradish peroxidase (1:2,500 dilution; Sigma) or goat anti-rabbit-conjugated horseradish peroxidase (1:2,500 dilution; Sigma) in 5% milk-TBST at room temperature for 1 h. Blots were washed in TBST then visualized using Western-C ECL substrate (Bio-Rad) on a ChemiDoc XRS+ System (Bio-Rad).

Histological analysis

Muscles were dissected and embedded in OCT or flash frozen using liquid-nitrogen-cooled isopentane. Subsequently, 10-μm sections were cut onto pretreated histological slides using a cryostat (Leica). Slides were washed in PBS and blocked in PBS supplemented with 5% BSA and 0.1% Triton X-100. Slides were stained with mouse anti-MANDYS106 (1:200 dilution; Millipore clone 2C6) and rabbit anti-laminin (1:300 dilution; Sigma L9393) in blocking buffer at room temperature for 1 h. Slides were washed 3× with PBS for 5 min, and goat anti-mouse immunoglobulin G2a (IgG2a), Alexa Fluor 594 (1:500 dilution; ThermoFisher A-21135) or goat anti-rabbit IgG (H+L), Alexa Fluor 488 (1:500 dilution; ThermoFisher A-11034) was applied with DAPI (1:1,000 dilution) at room temperature for 1 h. Slides were washed and mounted with ProLong Gold Antifade Mountant (Invitrogen) and imaged with a Zeiss AxioObserve 7 microscope. Total fibers (anti-laminin) were counted using the analyze particles function on ImageJ,[74] and human dystrophin-positive fibers (anti-MANDYS106) were manually counted from a series of 5 randomized images for each sample. Percent dystrophin-positive fibers was calculated as dystrophin-positive fibers divided by the total fibers for each image. p values were calculated by nested global one-way ANOVA with Tukey post hoc multiple comparisons tests.

Off-target analysis

CIRCLE-seq libraries[49] were generated as previously described.[75] Approximately 50–100 μg of HEK293T gDNA was used to generate circles for each reaction. Using a Diagenode Bioruptor XL sonicator at 4°C, gDNA was sonicated to an average size of approximately 50 bp, with a visible range of 200–1,000 bp, as determined by agarose gel electrophoresis. The enzymatic procedure to generate circles was carried out as previously described.[49] For the *in vitro* digest of the circles, gRNAs were synthesized from IDT and SaCas9 was purchased from Applied Biological Materials. Library production was carried out as previously described for CHANGE-seq.[50] Libraries were quantified by the qPCR-based KAPA Library Quantification Kit (KAPA Biosystems), pooled, and sequenced with 150-bp paired-end reads on an Illumina NextSeq instrument. Read counts were obtained using previously described methods and software for CHANGE-seq.[50] The following parameters were used for running the analysis pipeline: read threshold of 4; window size of 3; mapq threshold of 50; start threshold of 1; gap threshold of 3; mismatch threshold of 6; and PAM of NNGRRN.[43]

Creatine kinase assay

Serum creatine kinase was measured using a Liquid Creatine Kinase Reagent set (Pointe Scientific) following the manufacturer's instructions. In brief, 5 μL of serum was diluted in 45 μL sterile PBS and incubated with reagent for 2 min at 37°C followed by absorbance measurements taken every minute for three readings using a nanodrop spectrophotometer set for 340-nm readings. Calculations for total creatine kinase in U/L were made according to the manufacturer's instructions.

Data and code availability

All custom code has been made available online (https://github.com/siyansusan/DMD_integration_analysis). All sequencing data, including analyzed read counts, used in this study have been deposited in the National Center for Biotechnology Information Sequence Read Archive (SRA) database (GSE173224). All other relevant raw data are available from the corresponding author on request.

Statistical analysis

All data were analyzed with four to six biological replicates and presented as mean ± SEM. All p values were calculated by global one-way ANOVA with Tukey post hoc tests ($\alpha = 0.05$).

SUPPLEMENTAL INFORMATION

Supplemental information can be found online at https://doi.org/10.1016/j.ymthe.2021.09.003.

ACKNOWLEDGMENTS

We thank C. Nelson, M. Sitton, K.T. McCullough, M. Gemberling, and L. Brown for technical assistance and helpful comments.

Schematics were created with BioRender.com. We thank the Duke University School of Medicine for the use of the Sequencing and Genomic Technologies Shared Resource, which provided Novaseq and Nextseq services. This work was supported by Sarepta Therapeutics; a Duke–Coulter Translational Partnership Grant; a Duke/UNC-Chapel Hill CTSA Consortium Collaborative Translational Research Award (NIH UL1TR002553); NIH grants R01AR069085, UG3AR075336, and U01EB028901; and the Office of the Assistant Secretary of Defense for Health Affairs, through the Duchenne Muscular Dystrophy Research Program under award W81XWH-15-1-0469. A.P.-O. was supported by a Pfizer-NCBiotech Distinguished Postdoctoral Fellowship. V.G. and J.N.R.-H. were supported by US National Science Foundation (NSF) Graduate Research Fellowships, and V.G. was supported by a NIH Biotechnology Training Grant (T32GM008555).

AUTHOR CONTRIBUTIONS

A.P.-O., V.G., and C.A.G. designed the experiments. A.P.-O., G.D., and A.A. assisted in AAV production. H.D. assisted in mouse breeding and genotyping. A.P.-O., V.G., J.D.B., S.L., and J.N.R.-H. performed the experiments. A.P.-O., V.G., J.D.B., S.L., W.H.M., and C.A.G. analyzed the data. A.P.-O. and C.A.G. wrote the manuscript with input from all authors.

DECLARATION OF INTERESTS

A.P.-O., V.G., J.N.R.-H., and C.A.G. are inventors on patent applications related to genome editing. C.A.G. is an advisor to Sarepta Therapeutics, Tune Therapeutics, Levo Therapeutics, and Iveric Bio and a co-founder of Tune Therapeutics, Element Genomics, and Locus Biosciences. A.A. is a co-founder and advisor to StrideBio and TorqueBio.

REFERENCES

1. Maeder, M.L., and Gersbach, C.A. (2016). Genome-editing technologies for gene and cell therapy. Mol. Ther. *24*, 430–446.
2. Jinek, M., Chylinski, K., Fonfara, I., Hauer, M., Doudna, J.A., and Charpentier, E. (2012). A programmable dual-RNA-guided DNA endonuclease in adaptive bacterial immunity. Science *337*, 816–821.
3. Mali, P., Yang, L., Esvelt, K.M., Aach, J., Guell, M., DiCarlo, J.E., Norville, J.E., and Church, G.M. (2013). RNA-guided human genome engineering via Cas9. Science *339*, 823–826.
4. Cong, L., Ran, F.A., Cox, D., Lin, S., Barretto, R., Habib, N., Hsu, P.D., Wu, X., Jiang, W., Marraffini, L.A., and Zhang, F. (2013). Multiplex genome engineering using CRISPR/Cas systems. Science *339*, 819–823.
5. Jinek, M., East, A., Cheng, A., Lin, S., Ma, E., and Doudna, J. (2013). RNA-programmed genome editing in human cells. eLife *2*, e00471.
6. Cho, S.W., Kim, S., Kim, J.M., and Kim, J.S. (2013). Targeted genome engineering in human cells with the Cas9 RNA-guided endonuclease. Nat. Biotechnol. *31*, 230–232.
7. Lombardo, A., Cesana, D., Genovese, P., Di Stefano, B., Provasi, E., Colombo, D.F., Neri, M., Magnani, Z., Cantore, A., Lo Riso, P., et al. (2011). Site-specific integration and tailoring of cassette design for sustainable gene transfer. Nat. Methods *8*, 861–869.
8. Sharma, R., Anguela, X.M., Doyon, Y., Wechsler, T., DeKelver, R.C., Sproul, S., Paschon, D.E., Miller, J.C., Davidson, R.J., Shivak, D., et al. (2015). In vivo genome editing of the albumin locus as a platform for protein replacement therapy. Blood *126*, 1777–1784.
9. Li, H., Haurigot, V., Doyon, Y., Li, T., Wong, S.Y., Bhagwat, A.S., Malani, N., Anguela, X.M., Sharma, R., Ivanciu, L., et al. (2011). In vivo genome editing restores haemostasis in a mouse model of haemophilia. Nature *475*, 217–221.
10. Lombardo, A., Genovese, P., Beausejour, C.M., Colleoni, S., Lee, Y.L., Kim, K.A., Ando, D., Urnov, F.D., Galli, C., Gregory, P.D., et al. (2007). Gene editing in human stem cells using zinc finger nucleases and integrase-defective lentiviral vector delivery. Nat. Biotechnol. *25*, 1298–1306.
11. Orthwein, A., Noordermeer, S.M., Wilson, M.D., Landry, S., Enchev, R.I., Sherker, A., Munro, M., Pinder, J., Salsman, J., Dellaire, G., et al. (2015). A mechanism for the suppression of homologous recombination in G1 cells. Nature *528*, 422–426.
12. Maresca, M., Lin, V.G., Guo, N., and Yang, Y. (2013). Obligate ligation-gated recombination (ObLiGaRe): custom-designed nuclease-mediated targeted integration through nonhomologous end joining. Genome Res. *23*, 539–546.
13. Cristea, S., Freyvert, Y., Santiago, Y., Holmes, M.C., Urnov, F.D., Gregory, P.D., and Cost, G.J. (2013). In vivo cleavage of transgene donors promotes nuclease-mediated targeted integration. Biotechnol. Bioeng. *110*, 871–880.
14. Suzuki, K., Tsunekawa, Y., Hernandez-Benitez, R., Wu, J., Zhu, J., Kim, E.J., Hatanaka, F., Yamamoto, M., Araoka, T., Li, Z., et al. (2016). In vivo genome editing via CRISPR/Cas9 mediated homology-independent targeted integration. Nature *540*, 144–149.
15. Bloomer, H., Smith, R.H., Hakami, W., and Larochelle, A. (2021). Genome editing in human hematopoietic stem and progenitor cells via CRISPR-Cas9-mediated homology-independent targeted integration. Mol. Ther. *29*, 1611–1624.
16. Fairclough, R.J., Wood, M.J., and Davies, K.E. (2013). Therapy for Duchenne muscular dystrophy: renewed optimism from genetic approaches. Nat. Rev. Genet. *14*, 373–378.
17. van Deutekom, J.C., and van Ommen, G.J. (2003). Advances in Duchenne muscular dystrophy gene therapy. Nat. Rev. Genet. *4*, 774–783.
18. Chamberlain, J.R., and Chamberlain, J.S. (2017). Progress toward gene therapy for Duchenne muscular dystrophy. Mol. Ther. *25*, 1125–1131.
19. Wang, B., Li, J., Fu, F.H., and Xiao, X. (2009). Systemic human minidystrophin gene transfer improves functions and life span of dystrophin and dystrophin/utrophin-deficient mice. J. Orthop. Res. *27*, 421–426.
20. Harper, S.Q., Hauser, M.A., DelloRusso, C., Duan, D., Crawford, R.W., Phelps, S.F., Harper, H.A., Robinson, A.S., Engelhardt, J.F., Brooks, S.V., and Chamberlain, J.S. (2002). Modular flexibility of dystrophin: implications for gene therapy of Duchenne muscular dystrophy. Nat. Med. *8*, 253–261.
21. Shin, J.H., Pan, X., Hakim, C.H., Yang, H.T., Yue, Y., Zhang, K., Terjung, R.L., and Duan, D. (2013). Microdystrophin ameliorates muscular dystrophy in the canine model of duchenne muscular dystrophy. Mol. Ther. *21*, 750–757.
22. Gregorevic, P., Blankinship, M.J., Allen, J.M., and Chamberlain, J.S. (2008). Systemic microdystrophin gene delivery improves skeletal muscle structure and function in old dystrophic mdx mice. Mol. Ther. *16*, 657–664.
23. Koppanati, B.M., Li, J., Reay, D.P., Wang, B., Daood, M., Zheng, H., Xiao, X., Watchko, J.F., and Clemens, P.R. (2010). Improvement of the mdx mouse dystrophic phenotype by systemic in utero AAV8 delivery of a minidystrophin gene. Gene Ther. *17*, 1355–1362.
24. Cirak, S., Arechavala-Gomeza, V., Guglieri, M., Feng, L., Torelli, S., Anthony, K., Abbs, S., Garralda, M.E., Bourke, J., Wells, D.J., et al. (2011). Exon skipping and dystrophin restoration in patients with Duchenne muscular dystrophy after systemic phosphorodiamidate morpholino oligomer treatment: an open-label, phase 2, dose-escalation study. Lancet *378*, 595–605.
25. Goemans, N.M., Tulinius, M., van den Akker, J.T., Burm, B.E., Ekhart, P.F., Heuvelmans, N., Holling, T., Janson, A.A., Platenburg, G.J., Sipkens, J.A., et al. (2011). Systemic administration of PRO051 in Duchenne's muscular dystrophy. N. Engl. J. Med. *364*, 1513–1522.
26. Nelson, C.E., Robinson-Hamm, J.N., and Gersbach, C.A. (2017). Genome engineering: a new approach to gene therapy for neuromuscular disorders. Nat. Rev. Neurol. *13*, 647–661.
27. Young, C.S., Hicks, M.R., Ermolova, N.V., Nakano, H., Jan, M., Younesi, S., Karumbayaram, S., Kumagai-Cresse, C., Wang, D., Zack, J.A., et al. (2016). A single

CRISPR-Cas9 deletion strategy that targets the majority of DMD patients restores dystrophin function in hiPSC-derived muscle cells. Cell Stem Cell *18*, 533–540.

28. Nelson, C.E., Hakim, C.H., Ousterout, D.G., Thakore, P.I., Moreb, E.A., Castellanos Rivera, R.M., Madhavan, S., Pan, X., Ran, F.A., Yan, W.X., et al. (2016). In vivo genome editing improves muscle function in a mouse model of Duchenne muscular dystrophy. Science *351*, 403–407.

29. Tabebordbar, M., Zhu, K., Cheng, J.K.W., Chew, W.L., Widrick, J.J., Yan, W.X., Maesner, C., Wu, E.Y., Xiao, R., Ran, F.A., et al. (2016). In vivo gene editing in dystrophic mouse muscle and muscle stem cells. Science *351*, 407–411.

30. Long, C., Amoasii, L., Mireault, A.A., McAnally, J.R., Li, H., Sanchez-Ortiz, E., Bhattacharyya, S., Shelton, J.M., Bassel-Duby, R., and Olson, E.N. (2016). Postnatal genome editing partially restores dystrophin expression in a mouse model of muscular dystrophy. Science *351*, 400–403.

31. Bengtsson, N.E., Hall, J.K., Odom, G.L., Phelps, M.P., Andrus, C.R., Hawkins, R.D., Hauschka, S.D., Chamberlain, J.R., and Chamberlain, J.S. (2017). Muscle-specific CRISPR/Cas9 dystrophin gene editing ameliorates pathophysiology in a mouse model for Duchenne muscular dystrophy. Nat. Commun. *8*, 14454.

32. Amoasii, L., Long, C., Li, H., Mireault, A.A., Shelton, J.M., Sanchez-Ortiz, E., McAnally, J.R., Bhattacharyya, S., Schmidt, F., Grimm, D., et al. (2017). Single-cut genome editing restores dystrophin expression in a new mouse model of muscular dystrophy. Sci. Transl. Med. *9*, eaan8081.

33. Min, Y.L., Chemello, F., Li, H., Rodriguez-Caycedo, C., Sanchez-Ortiz, E., Mireault, A.A., McAnally, J.R., Shelton, J.M., Zhang, Y., Bassel-Duby, R., and Olson, E.N. (2020). Correction of three prominent mutations in mouse and human models of Duchenne muscular dystrophy by single-cut genome editing. Mol. Ther. *28*, 2044–2055.

34. Bengtsson, N.E., Tasfaout, H., Hauschka, S.D., and Chamberlain, J.S. (2021). Dystrophin gene-editing stability is dependent on dystrophin levels in skeletal but not cardiac muscles. Mol. Ther. *29*, 1070–1085.

35. Amoasii, L., Hildyard, J.C.W., Li, H., Sanchez-Ortiz, E., Mireault, A., Caballero, D., Harron, R., Stathopoulou, T.R., Massey, C., Shelton, J.M., et al. (2018). Gene editing restores dystrophin expression in a canine model of Duchenne muscular dystrophy. Science *362*, 86–91.

36. Kabadi, A.M., Ousterout, D.G., Hilton, I.B., and Gersbach, C.A. (2014). Multiplex CRISPR/Cas9-based genome engineering from a single lentiviral vector. Nucleic Acids Res. *42*, e147.

37. Ousterout, D.G., Kabadi, A.M., Thakore, P.I., Perez-Pinera, P., Brown, M.T., Majoros, W.H., Reddy, T.E., and Gersbach, C.A. (2015). Correction of dystrophin expression in cells from Duchenne muscular dystrophy patients through genomic excision of exon 51 by zinc finger nucleases. Mol. Ther. *23*, 523–532.

38. Li, H.L., Fujimoto, N., Sasakawa, N., Shirai, S., Ohkame, T., Sakuma, T., Tanaka, M., Amano, N., Watanabe, A., Sakurai, H., et al. (2015). Precise correction of the dystrophin gene in duchenne muscular dystrophy patient induced pluripotent stem cells by TALEN and CRISPR-Cas9. Stem Cell Reports *4*, 143–154.

39. Phelps, S.F., Hauser, M.A., Cole, N.M., Rafael, J.A., Hinkle, R.T., Faulkner, J.A., and Chamberlain, J.S. (1995). Expression of full-length and truncated dystrophin minigenes in transgenic mdx mice. Hum. Mol. Genet. *4*, 1251–1258.

40. 't Hoen, P.A.C., de Meijer, E.J., Boer, J.M., Vossen, R.H.A.M., Turk, R., Maatman, R.G.H.J., Davies, K.E., van Ommen, G.-J.B., van Deutekom, J.C.T., and den Dunnen, J.T. (2008). Generation and characterization of transgenic mice with the full-length human DMD gene. J. Biol. Chem. *283*, 5899–5907.

41. Young, C.S., Mokhonova, E., Quinonez, M., Pyle, A.D., and Spencer, M.J. (2017). Creation of a novel humanized dystrophic mouse model of Duchenne muscular dystrophy and application of a CRISPR/Cas9 gene editing therapy. J. Neuromuscul. Dis. *4*, 139–145.

42. Veltrop, M., van Vliet, L., Hulsker, M., Claassens, J., Brouwers, C., Breukel, C., van der Kaa, J., Linssen, M.M., den Dunnen, J.T., Verbeek, S., et al. (2018). A dystrophic Duchenne mouse model for testing human antisense oligonucleotides. PLoS ONE *13*, e0193289.

43. Ran, F.A., Cong, L., Yan, W.X., Scott, D.A., Gootenberg, J.S., Kriz, A.J., Zetsche, B., Shalem, O., Wu, X., Makarova, K.S., et al. (2015). In vivo genome editing using Staphylococcus aureus Cas9. Nature *520*, 186–191.

44. Bae, S., Park, J., and Kim, J.S. (2014). Cas-OFFinder: a fast and versatile algorithm that searches for potential off-target sites of Cas9 RNA-guided endonucleases. Bioinformatics *30*, 1473–1475.

45. Friedland, A.E., Baral, R., Singhal, P., Loveluck, K., Shen, S., Sanchez, M., Marco, E., Gotta, G.M., Maeder, M.L., Kennedy, E.M., et al. (2015). Characterization of Staphylococcus aureus Cas9: a smaller Cas9 for all-in-one adeno-associated virus delivery and paired nickase applications. Genome Biol. *16*, 257.

46. Zincarelli, C., Soltys, S., Rengo, G., and Rabinowitz, J.E. (2008). Analysis of AAV serotypes 1-9 mediated gene expression and tropism in mice after systemic injection. Mol. Ther. *16*, 1073–1080.

47. Nelson, C.E., Wu, Y., Gemberling, M.P., Oliver, M.L., Waller, M.A., Bohning, J.D., Robinson-Hamm, J.N., Bulaklak, K., Castellanos Rivera, R.M., Collier, J.H., et al. (2019). Long-term evaluation of AAV-CRISPR genome editing for Duchenne muscular dystrophy. Nat. Med. *25*, 427–432.

48. Giannoukos, G., Ciulla, D.M., Marco, E., Abdulkerim, H.S., Barrera, L.A., Bothmer, A., Dhanapal, V., Gloskowski, S.W., Jayaram, H., Maeder, M.L., et al. (2018). UDiTaS™, a genome editing detection method for indels and genome rearrangements. BMC Genomics *19*, 212.

49. Tsai, S.Q., Nguyen, N.T., Malagon-Lopez, J., Topkar, V.V., Aryee, M.J., and Joung, J.K. (2017). CIRCLE-seq: a highly sensitive in vitro screen for genome-wide CRISPR-Cas9 nuclease off-targets. Nat. Methods *14*, 607–614.

50. Lazzarotto, C.R., Malinin, N.L., Li, Y., Zhang, R., Yang, Y., Lee, G., Cowley, E., He, Y., Lan, X., Jividen, K., et al. (2020). CHANGE-seq reveals genetic and epigenetic effects on CRISPR-Cas9 genome-wide activity. Nat. Biotechnol. *38*, 1317–1327.

51. Aartsma-Rus, A., Fokkema, I., Verschuuren, J., Ginjaar, I., van Deutekom, J., van Ommen, G.J., and den Dunnen, J.T. (2009). Theoretic applicability of antisense-mediated exon skipping for Duchenne muscular dystrophy mutations. Hum. Mutat. *30*, 293–299.

52. Nelson, C.E., and Gersbach, C.A. (2019). In Muscle Gene Therapy, D. Duan and J.R. Mendell, eds. (Springer International), pp. 383–403.

53. Monaco, A.P., Neve, R.L., Colletti-Feener, C., Bertelson, C.J., Kurnit, D.M., and Kunkel, L.M. (1986). Isolation of candidate cDNAs for portions of the Duchenne muscular dystrophy gene. Nature *323*, 646–650.

54. van Putten, M., Hulsker, M., Nadarajah, V.D., van Heiningen, S.H., van Huizen, E., van Iterson, M., Admiraal, P., Messemaker, T., den Dunnen, J.T., 't Hoen, P.A., and Aartsma-Rus, A. (2012). The effects of low levels of dystrophin on mouse muscle function and pathology. PLoS ONE *7*, e31937.

55. van Putten, M., van der Pijl, E.M., Hulsker, M., Verhaart, I.E., Nadarajah, V.D., van der Weerd, L., and Aartsma-Rus, A. (2014). Low dystrophin levels in heart can delay heart failure in mdx mice. J. Mol. Cell. Cardiol. *69*, 17–23.

56. van Putten, M., Hulsker, M., Young, C., Nadarajah, V.D., Heemskerk, H., van der Weerd, L., 't Hoen, P.A., van Ommen, G.J., and Aartsma-Rus, A.M. (2013). Low dystrophin levels increase survival and improve muscle pathology and function in dystrophin/utrophin double-knockout mice. FASEB J. *27*, 2484–2495.

57. Chew, W.L., Tabebordbar, M., Cheng, J.K., Mali, P., Wu, E.Y., Ng, A.H., Zhu, K., Wagers, A.J., and Church, G.M. (2016). A multifunctional AAV-CRISPR-Cas9 and its host response. Nat. Methods *13*, 868–874.

58. Maeder, M.L., Stefanidakis, M., Wilson, C.J., Baral, R., Barrera, L.A., Bounoutas, G.S., Bumcrot, D., Chao, H., Ciulla, D.M., DaSilva, J.A., et al. (2019). Development of a gene-editing approach to restore vision loss in Leber congenital amaurosis type 10. Nat. Med. *25*, 229–233.

59. Li, A., Tanner, M.R., Lee, C.M., Hurley, A.E., De Giorgi, M., Jarrett, K.E., Davis, T.H., Doerfler, A.M., Bao, G., Beeton, C., and Lagor, W.R. (2020). AAV-CRISPR gene editing is negated by pre-existing immunity to Cas9. Mol. Ther. *28*, 1432–1441.

60. Madigan, V.J., and Asokan, A. (2016). Engineering AAV receptor footprints for gene therapy. Curr. Opin. Virol. *18*, 89–96.

61. Himeda, C.L., Chen, X., and Hauschka, S.D. (2011). Design and testing of regulatory cassettes for optimal activity in skeletal and cardiac muscles. Methods Mol. Biol. *709*, 3–19.

62. McVey, M., and Lee, S.E. (2008). MMEJ repair of double-strand breaks (director's cut): deleted sequences and alternative endings. Trends Genet. *24*, 529–538.

63. Nakade, S., Tsubota, T., Sakane, Y., Kume, S., Sakamoto, N., Obara, M., Daimon, T., Sezutsu, H., Yamamoto, T., Sakuma, T., and Suzuki, K.T. (2014). Microhomology-mediated end-joining-dependent integration of donor DNA in cells and animals using TALENs and CRISPR/Cas9. Nat. Commun. *5*, 5560.

64. Sakuma, T., Nakade, S., Sakane, Y., Suzuki, K.T., and Yamamoto, T. (2016). MMEJ-assisted gene knock-in using TALENs and CRISPR-Cas9 with the PITCh systems. Nat. Protoc. *11*, 118–133.

65. Yao, X., Wang, X., Liu, J., Hu, X., Shi, L., Shen, X., Ying, W., Sun, X., Wang, X., Huang, P., and Yang, H. (2017). CRISPR/Cas9 - mediated precise targeted integration in vivo using a double cut donor with short homology arms. EBioMedicine *20*, 19–26.

66. Yao, X., Wang, X., Liu, J., Shi, L., Huang, P., and Yang, H. (2018). CRISPR/Cas9-mediated targeted integration in vivo using a homology-mediated end joining-based strategy. J. Vis. Exp. 56844.

67. Suzuki, K., Yamamoto, M., Hernandez-Benitez, R., Li, Z., Wei, C., Soligalla, R.D., Aizawa, E., Hatanaka, F., Kurita, M., Reddy, P., et al. (2019). Precise in vivo genome editing via single homology arm donor mediated intron-targeting gene integration for genetic disease correction. Cell Res. *29*, 804–819.

68. Li, H., Yang, Y., Hong, W., Huang, M., Wu, M., and Zhao, X. (2020). Applications of genome editing technology in the targeted therapy of human diseases: mechanisms, advances and prospects. Signal Transduct. Target. Ther. *5*, 1.

69. Mamchaoui, K., Trollet, C., Bigot, A., Negroni, E., Chaouch, S., Wolff, A., Kandalla, P.K., Marie, S., Di Santo, J., St Guily, J.L., et al. (2011). Immortalized pathological human myoblasts: towards a universal tool for the study of neuromuscular disorders. Skelet. Muscle *1*, 34.

70. Guschin, D.Y., Waite, A.J., Katibah, G.E., Miller, J.C., Holmes, M.C., and Rebar, E.J. (2010). A rapid and general assay for monitoring endogenous gene modification. Methods Mol. Biol. *649*, 247–256.

71. Springer, M.L., Rando, T.A., and Blau, H.M. (2002). Gene delivery to muscle. Curr. Protoc. Hum. Genet. *Chapter 13*, Unit13.4.

72. Gombash Lampe, S.E., Kaspar, B.K., and Foust, K.D. (2014). Intravenous injections in neonatal mice. J. Vis. Exp. e52037.

73. Picelli, S., Björklund, A.K., Reinius, B., Sagasser, S., Winberg, G., and Sandberg, R. (2014). Tn5 transposase and tagmentation procedures for massively scaled sequencing projects. Genome Res. *24*, 2033–2040.

74. Schindelin, J., Arganda-Carreras, I., Frise, E., Kaynig, V., Longair, M., Pietzsch, T., Preibisch, S., Rueden, C., Saalfeld, S., Schmid, B., et al. (2012). Fiji: an open-source platform for biological-image analysis. Nat. Methods *9*, 676–682.

75. Kocak, D.D., Josephs, E.A., Bhandarkar, V., Adkar, S.S., Kwon, J.B., and Gersbach, C.A. (2019). Increasing the specificity of CRISPR systems with engineered RNA secondary structures. Nat. Biotechnol. *37*, 657–666.